Electrochemical Preparation of Luminescent Graphene Quantum Dots from Multiwalled Carbon Nanotubes

Dhanraj B. Shinde[a] and Vijayamohanan K. Pillai*[a, b]

Abstract: Green luminescent, graphene quantum dots (GQDs) with a uniform size of 3, 5, and 8.2($\pm$0.3) nm in diameter were prepared electrochemically from MWCNTs in propylene carbonate by using $LiClO_4$ at 90°C, whereas similar particles of 23($\pm$2) nm were obtained at 30°C under identical conditions. Both these sets of GQDs displayed a remarkable quantum efficiency of 6.3 and 5.1%, respectively. This method offers a novel strategy to syn- thesise size-tunable GQDs as evidenced by multiple characterisation techniques like transmission and scanning electron microscopy, atomic force microscopy, Raman spectroscopy and X-ray diffraction (XRD). Photoluminescence of these GQDs can be tail- ored by size variation through a systematic change in key process parameters, like diameter of carbon nanotube, electric field, concentration of supporting electrolyte and temperature. GQDs are promising candidates for a variety of applications, such as biomarkers, nanoelectronic devices and chemosensors due to their unique features, like high photostability, biocompatibility, nontoxicity and tunable solubility in water.

Keywords: electrochemical synthesis · graphene · nanostructures · photoluminescence · quantum dots

Introduction

Graphene has attracted enormous attention because of its unique and novel electronic properties, which could facilitate numerous promising applications.[1–3] However, graphene is a zero band gap semiconductor, which renders its electronic and optoelectronic properties almost impossible to use for device applications.[4] Interestingly, this zero band gap material has been more recently engineered to form graphene nanoribbons[5] (GNRs) and graphene quantum dots[6–9] (GQDs), which reveal several significant properties like high mobility and ballistic transport[10] due to quantum confinement[11] and edge effects. The strong and tunable luminescence of GQDs is especially attractive because of the promising applications in light emitting diodes,[12] electroluminescence,[13] organic photovoltaic devices,[14] biological labelling[15,16] and medicine.[17]

Despite all these important applications, a simple method to produce size-selective GQDs in high yield is a daunting challenge. For example, Pan and co-workers presented a hydrothermal method for cutting pre-oxidised graphene sheets into GQDs[18] (ca. 10 nm) displaying blue luminescence due to a large edge effect. Also, Qu et al. reported the synthesis of GQDs from graphene oxide using cyclic voltammetry (CV) within the potential window ± 3 V with phosphate buffer solution.[19] Ding et al. reported the synthesis of nanocrystals from multiwalled carbon nanotubes (MWCNTs) with a wide size distribution, although most of the MWCNTs became entangled together with the unreacted parts exhibiting swollen and curled features.[20] Recently Mullen et al. reported the synthesis of GQDs of larger size by a bottom-up approach using polycyclic aromatic hydrocarbons,[21] but with no control on edge states. There are also methods based on electron beam lithography[22] and ruthenium catalysed C_{60} transformation[23] for GQD synthesis. Many of these methods are limited by the requirement for special equipment and the yield is limited by expensive starting materials. For example, methods that are based on graphene oxide as a starting material need toxic chemical treatments for its synthesis. Hence, it would be easier to achieve size-controlled synthesis if the starting material already had smaller domain structures of sp^2 carbon, like that in MWCNTs. So electrochemical methods[24] with a potentiostatic control with selective oxidation followed by reduction would be beneficial to obtain GQDs by precise control of the size and shape. Also, the presented method is unique, since an accurate control of potential (especially by potentiostatic techniques) enables a means of monitoring the size of GQDs, and more importantly, offers the opportunity to achieve large scale (using large area electrodes) synthesis. Moreover, the earlier work concerned only graphene nanoribbons[25] as there was no quantum dot formation in aqueous media.

We have recently reported electrochemical unzipping of CNTs by a two-step process, producing high quality GNRs with smooth edges and fewer defects.[25] Subsequent experi-

[a] D. B. Shinde, Prof. V. K. Pillai
Physical/Materials Chemistry Division
National Chemical Laboratory
Homi Bhabha Road, Pune-411008 (India)
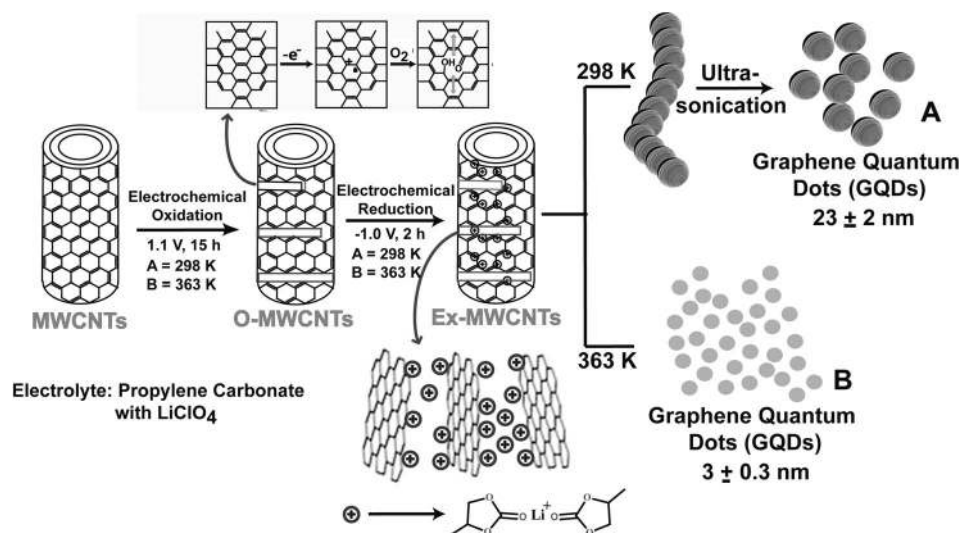E-mail: vk.pillai@ncl.res.in

[b] Prof. V. K. Pillai
Central Electrochemical Research Institute
Karaikudi 630006 (India)

ments to understand the effect of ionic strength and pH in aqueous media unravelled the critical role of oxygen in opening CNTs. However, when similar experiments were conducted in non-aqueous media, like propylene carbonate, we could, surprisingly, obtain GQDs, unlike that of GNRs in aqueous media. More specifically, sustained oxidation (15 h) of MWCNTs in propylene carbonate with LiClO$_4$ at 1 V followed by reduction yielded discrete spherical particles of GQDs presumably due to lateral unzipping. These GQDs are characterised by transmission and scanning electron microscopy, atomic force microscopy (AFM), Raman spectroscopy and X-ray diffraction (XRD), and their remarkable size-dependant light-emitting behaviour is highlighted in this article to enable promising applications.

Results and Discussion

Scheme 1 represents our two-step process for the electrochemical transformation of MWCNTs to GQDs. The first
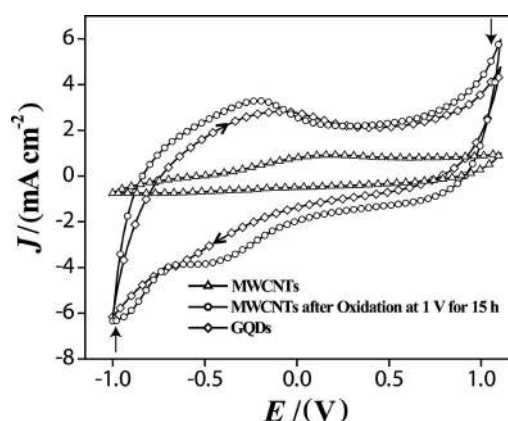

Figure 1. Cyclic voltammograms of MWCNTs, before and after oxidation at 1 V (vs. Pt quasi-reference electrode) for 15 h and GQDS in a potential window of −1 to 1.1 V at 50 mV s^{-1} in propylene carbonate with LiClO$_4$ (3 mM) as supporting electrolyte. Regions marked with arrows indicate the potential where CNTs have been selectively oxidised or reduced.

Scheme 1. Schematic representation of various processing stages involved in the preparation of photoluminescent GQDs from MWCNTs by this electrochemical approach.

step comprises of applying a typical anodic potential of 1 V versus Pt QRE (quasi reference electrode) to the MWCNT-coated working electrode in propylene carbonate with LiClO$_4$, in which the applied electric field initiates the breaking of sp^2 carbon atoms. More interesting is the variation with respect to the time of oxidation and also changes in the second step after applying a potential of −1 V versus QRE. This is attributed to the intercalation of Li$^+$/propylene carbonate complexes resulting in exfoliation of oxidised MWCNTs, facilitating the formation of size-tunable GQDs.

Figure 1 shows superimposed cyclic voltammograms of MWCNs before and after oxidation at 1 V for 15 h, and GQDs in a potential window of −1 to 1.1 V at 50 mV s^{-1} in propylene carbonate with LiClO$_4$ (3 mM) as supporting elec-

trolyte. MWCNTs are electrochemically silent, except for a small increase in non-Faradaic current with cycle number, and this subtle morphological changes is known.[25] By keeping the potential at 1 V for 7, 11 and 15 h, MWCNTs undergo oxidative cleavage, and interestingly, at the end, the open circuit potential (OCP) also increases by 54, 67 and 73 mV, respectively, clearly revealing the formation of oxidised species along with perhaps many topological defects. A similar shift in OCP has been observed in aqueous media presumably due to oxidative unzipping, and IR studies indicate the presence of residual oxygen containing species.[25] Although 15 h oxidation could generate ultrathin, two dimensional (1–3 atomic layer thick), monodispersed, high quality GQDs, the efficiency was low due to parasitic reactions during sustained oxidation. The number of Coulombs utilised has been estimated by integrating the I–t curves, and typical curves (for 5 min) are shown in Figure S5 in the Supporting Information. There are several steps in the mechanism involving oxidative C–C cleavage and the details are under investigation. However, further reduction causes a diminution in charge storage (area) although conductivity measurement indicates enhancement in carrier concentration (Figure S2 in the Supporting Information).

Figure 2 shows typical TEM images of GQDs prepared from MWCNTs at 30 °C by the two-step electrochemical
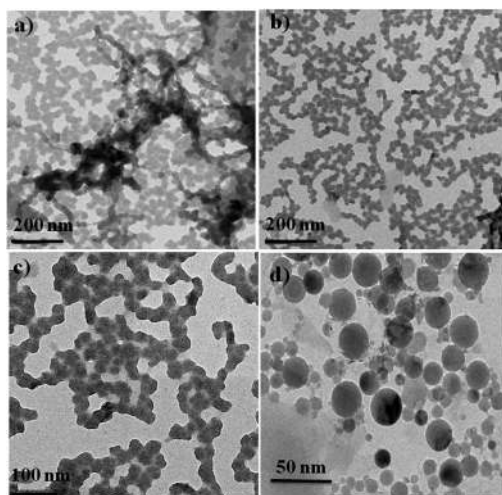
Figure 2. a), b) Typical TEM images of GQDs synthesised at 30 °C by using oxidation at 1 V for 7 h followed by reduction at −1 V; c) GQDs prepared by oxidation at 1 V for 11 h, followed by reduction at −1 V; d) GQDs with different levels of sonication prepared at 1 V for 15 h followed by reduction at −1 V.

process. Figure 2a corresponds to interconnected quantum dots obtained after oxidation at 1 V for 7 h followed by subsequent reduction at −1 V for 2 h. Figure 2b and c correspond to swelled interconnected GQDs obtained by oxidation at 1 V for 11 h, and show two different magnifications; Figure 2d shows complete transformation of 40–50 nm diameter MWCNTs to GQDs after oxidation at 1 V for 15 h. The TEM images in Figure 2 suggest more or less monodispersed GQDs as evidenced in the histogram in Figure S3 in the Supporting Information, which exhibits the analysis of more than 100 spherical particles, verified by analysing two different samples. Figure 3 shows TEM images of monodispersed GQDs with average sizes of 3(±0.3), 5(±0.3) and 8.2 (±0.3) nm prepared at 90 °C by using oxidation at 1 V for 15, 11 and 7 h, respectively. It indicates that the time of oxidation plays an important role in controlling the size of GQDs; the longer the oxidation time, the smaller are the resulting GQDs. The GQDs were observed to be transparent and stable under electron beam irradiation. More significantly, these GQDs show a d-spacing of 0.33 and 0.242 nm corresponding to (002) and (1120) lattice planes; this is in excellent agreement with what is known for GQDs prepared by using other routes[17,18] (Figure 3g). Figure 3h shows a selected-area electron diffraction (SAED) pattern.

Accurate information about the change in both height and lateral dimensions was obtained from AFM measurements (Figure 4a), which revealed a size distribution between 3–4 nm with 3.2 nm mean diameter. Interestingly, this topographic height between 1–2 nm also suggests the presence of 1–3 layers of graphene in each individual GQD. This suggests high quality as proved from conductivity data (Figure S2 in the Supporting Information) and these GQDs are much smaller than those prepared by other methods.[3,19] Figure 4b and c display AFM images and their corresponding height profiles for samples prepared by using a potential
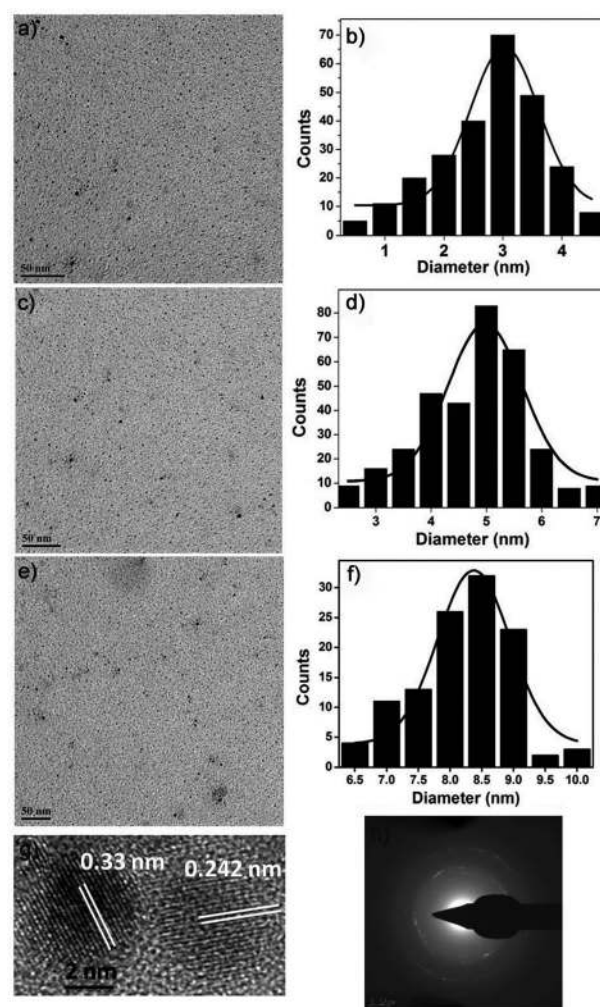

Figure 3. Panel of TEM images correspond to synthesis at 90 °C by using oxidation at 1 V for: a) 15, c) 11, and e) 7 h, with their size distribution histograms (b, d, f, respectively). g) Fringe patterns of GQDs, and h) SAED pattern of GQDs (8.2(±0.3) nm) displaying (002) as prominent plane.

of 1 V at 90 °C for 11 and 7 h, respectively; this resulted in different sized (4–5 and 6–7 nm, height varying from 3–5 nm) monodispersed GQDs. GQDs synthesised at 30 °C reveal long quantum dot chains (1 μm) with straight edges and widths ranging from 30 to 40 nm and height in the range of 18–24 nm (Figure 4d); this confirms a clear transformation of MWCNTs to GQDs with different yields (30–38 %). Figure S4 in the Supporting Information shows the SEM image of an as-prepared sample of GQDs at 30 °C.

In order to explore the optical properties of as-synthesised GQDs, we also carried out UV/Vis absorption and normal photoluminescence (PL) measurements. For the UV/Vis absorption there is no clear peak except for an extended absorption edge (Figure 5a). However, the PL spectrum interestingly shows a broad excitation-dependent peak, similar to Si nanocrystals, perhaps due to the distribution of different emissive sites.[26] More specifically, the UV/Vis absorption spectrum of GQDs in water with solubility of 1–
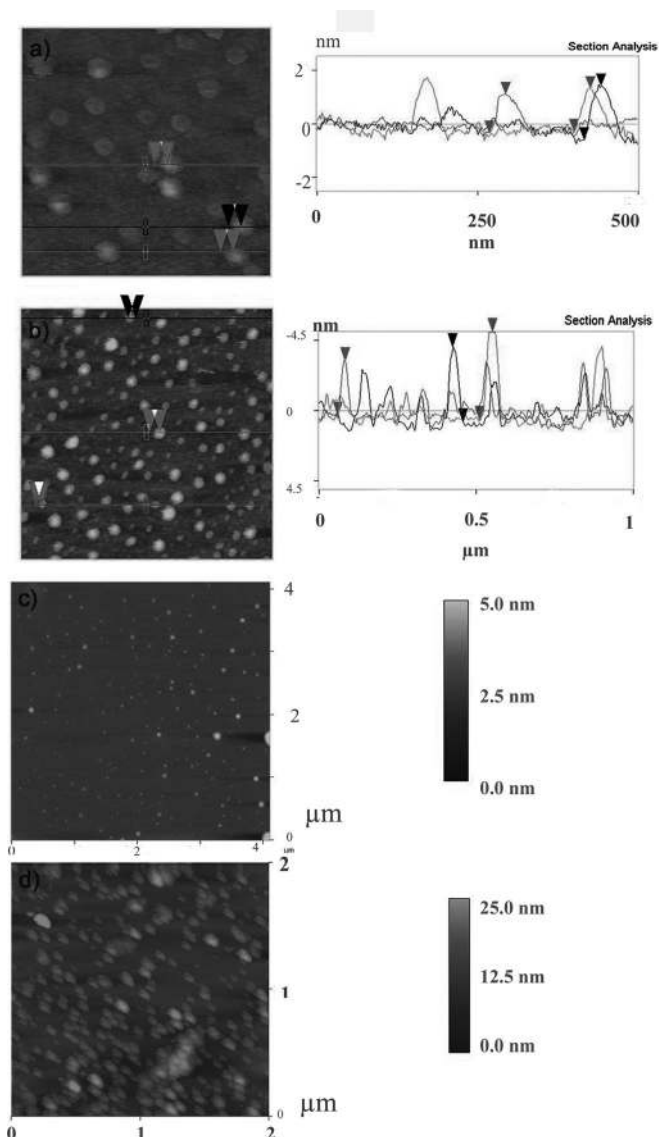
Figure 4. AFM images of monodispersed GQDs corresponding to synthesis at 90 °C by using oxidation at 1 V for: a) 15, b) 11, and c) 7 h, followed by reduction at −1 V for 2 h for each, with the corresponding height profiles. d) Synthesis at 30 °C by using oxidation at 1 V for 15 h showing transformation of MWCNTs to GQDs with heights of 15–20 nm.
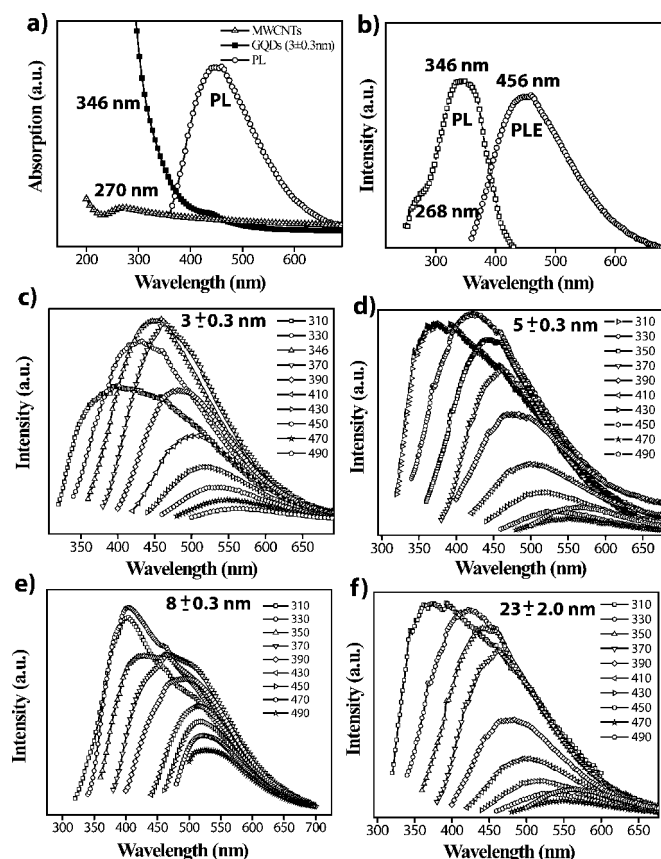

Figure 5. a) UV/Vis absorption and PL (346 nm excitation) spectra of GQDs dispersed in water; b) PLE spectrum with the detection wavelength of 440 nm and PL spectrum excited at 346 nm. c)–f) PL spectra at different excitation wavelengths for 3(±0.3), 5(±0.3), 8.2(±0.3) and 23(±2) nm GQDs.

2 µg mL⁻¹ shows an absorption band at about 346 nm (Figure 3 a) whereas upon excitation near the absorption band, the PL spectrum shows a strong peak at 456 nm (Figure 5 b). This is in excellent agreement with the emission spectra of the GQDs synthesised hydrothermally, and the origin of the luminescence could be ascribed to the presence of free zigzag sites[27] with a carbene-like triplet ground state. GQDs, especially in the range of 3–23 nm, contribute predominantly to free zigzag sites.[17] Interestingly, the carbene ground state multiplicity is related to the energy difference (ΔE) between σ and π orbitals. It has been determined earlier that for a triplet ground state, ΔE should be below 1.5 eV because the triplet carbenes are most common at zigzag edges.

Photoluminescence excitation spectra (PLE) for the 3-(±0.3) nm GQDs reveal two distinct electronic transitions at 268 nm (4.62 eV) and 346 nm (3.58 eV), which could be attributed to transitions from HOMO (σ and π orbitals) to LUMO. This ΔE (1.04 eV) is also interestingly suitable for triplet carbene according to the Hoffman rule.[18,27,28] However, in sharp contrast to the blue luminescence of GQDs synthesised hydrothermally, the electrochemically synthesised GQDs excited at 346 nm emit a green luminescence (Figure S6 in the Supporting Information), which could presumably be attributed to the effect of bigger size and also due to different surface functional groups (Figure 6). Interestingly, the quantum yields are found to be 5.1–6.3 % (Table S1 in the Supporting Information) when calibrated against quinine sulfate,[29] which is indeed better than that of GQDs prepared by independent means (3.8 %).[21] This is also comparable to the observations of Ding et al. (6.4 %)[20] and signifies the utility of these GQDs as promising candidates for biolabelling and optoelectronic applications. Although luminescence mechanism of all GQDs appear to be similar, subtle changes occur since the total percentage of free zigzag edges might contribute variably as evidenced by the increase in the quantum yield from 5.1 to 6.3 % and red
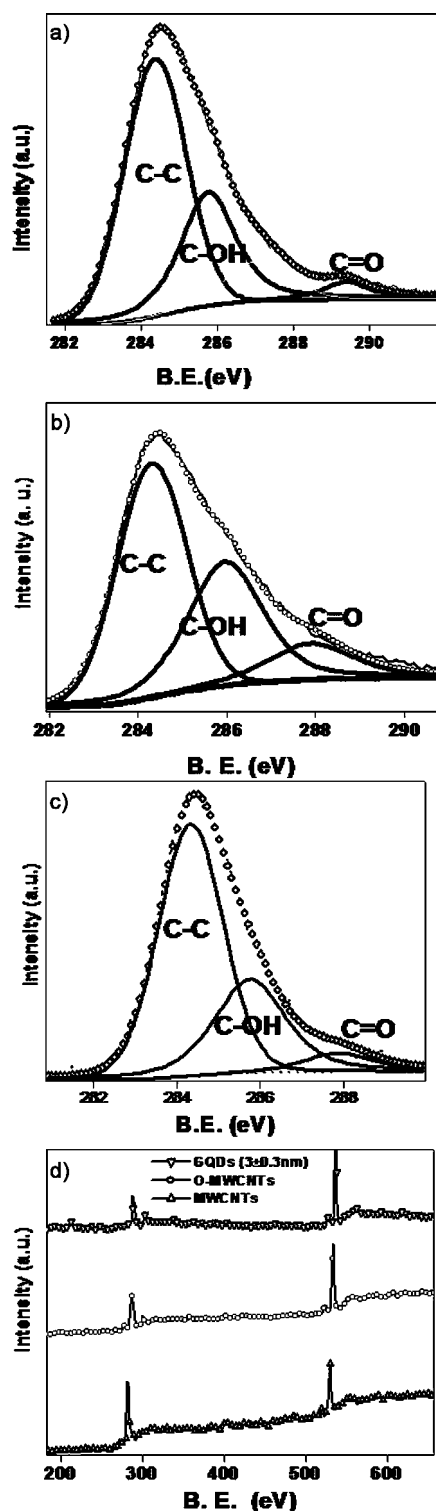
Figure 6. X-ray photoelectron spectra of C1s core level: a) MWCNT, b) oxidised MWCNT, c) GQDs (3(±0.3) nm), and d) complete XPS spectra showing percentage of carbon and oxygen; squares represent the experimental data, thick lines represent the fitting data for overall signal and the fitted lines are the deconvoluted individual peaks for different environments of carbon.

shift in the optimal emission wavelength (Figure 5c–f). Figure S1 in the Supporting Information displays PLE spectra

of four different samples of GQDs and Figure S7 in the Supporting Information corresponds to the size of GQDs and optimal emission wavelength.

Raman spectroscopy is a powerful and non-destructive tool for distinguishing between different types of ordered and disordered bonding environments of sp^2 and sp^3 hybridised carbon.[30,31] Normally in carbon nanostructures, the G band is assigned to the E_{2g} phonon of sp^2 carbon atoms, whereas the D band corresponds to the extent of defects.[32] In Figure 7a, the intensity of the D band at 1329 cm^{-1} for
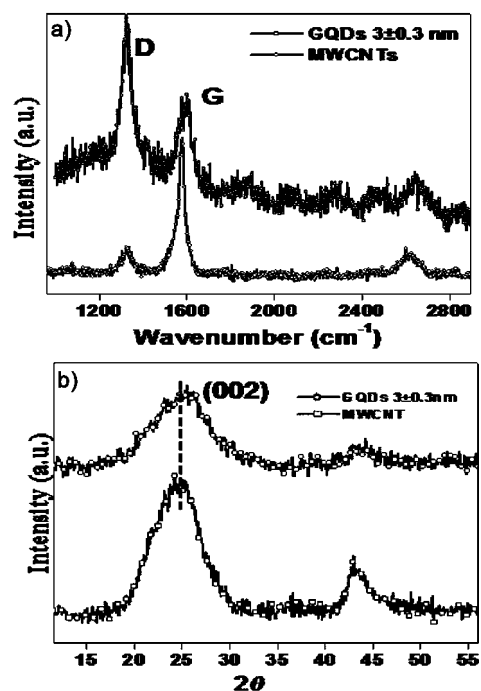

Figure 7. Comparison of: a) Raman spectra, and b) powder XRD patterns of MWCNTs and GQDs prepared by the two-step electrochemical method.

MWCNTs increases substantially; this indicates a possible decrease in the size of in-plane sp^2 domains due to oxidation. As seen in the case of pristine MWCNTs, the intensity of the D band is low, suggesting excellent quality of the starting materials.[5] After the electrochemical oxidation, the intensity of the D band is considerably enhanced along with a concomitant decrease in the intensity of the G band; this clearly reveals that the oxidation has been completed as confirmed by the observation of a high ratio of I_D/I_G bands. This type of electrochemically unzipped MWCNTs after 15 h typically show an I_D/I_G ratio of (1.23), suggesting edge effect as the central cause of fluorescence. These Raman results are in excellent agreement with the structural data from XRD of our GQDs.[30] Figure 7b shows a comparison of the XRD pattern of MWCNTs and GQDs. As the crystalline size of 11.4 nm inferred from the full width of half maximum (FWHM) of the broader (002) peak centred at 26.8° indicates, there are more active sites on GQDs with a d-spacing of 3.30 Å (Figure 6); this reveals the compactness of the structure compared to that of MWCNTs.

XPS data are invaluable for discriminating between MWCNTs, oxidised MWCNTs and GQDs and are used to calculate surface oxidation quantitatively.[33] In the XPS of carbon (C1s) the C−C binding energies were 284.51, 283.59 and 284.49 eV for MWCNTs, oxidised MWCNTs and GQDs, respectively. A decrease in intensity and binding energy (B.E.) value of C−C in Figure 6b is assigned to the weakening of the C−C bond and the introduction of a more sp^3 character in MWCNTs. The peak at 285.9 eV corresponds to C−O and that at 287 eV is assigned to carbonyl groups (C=O). Upon reduction by applying a negative potential at −1 V for 2 h the peaks at 285.9 and 287 eV decrease indicating a slight deoxygenation followed by exfoliation due to intercalation of Li/propylene carbonate resulting in GQDs. The oxygen to carbon ratios in Figure 6d for MWCNTs, oxidised MWCNTs and GQDs are 0.05, 0.14 and 0.10, respectively.

One of the major problems of these GQDs for cellular and molecular imaging applications is their Li content; it is also important to understand any decisive role played by lithium cation intercalation during the mechanism of GQD formation. Accordingly, several experiments were conducted by using tetrabutyl ammonium perchlorate instead of lithium perchlorate and the anion and solvent dependence was investigated. All results indicate that cation/propylene carbonate complexes are primarily responsible for the high-yield exfoliation of oxidised MWCNTs to produce GQDs.[34] A possible mechanism for this transformation of MWCNTs to GQDs could be formulated based on the above results (Scheme 1) assuming vertical unzipping in contrast to longitudinal unzipping in the aqueous case. However, considering the fact that C−C cleavage can initiate at topological defects with enough strain (due to high field gradients), transverse splitting of the tube walls could be facilitated at these transient openings. According to this mechanism, the field gradient on the edges of split MWCNTs could overcome the van der Waals force between the graphene layers. These GQDs are expected to be generated by the oxidation of the C−C bond, following the exfoliation of oxidised MWCNTs. The fragmentation could be initiated by the synergetic effect of intercalation of Li and propylene carbonate in the turbostratic structure under electric field,[35] facilitated by the considerable interlayer stress. Solid state NMR spectroscopy and Raman imaging experiments are in progress to unravel distinct steps involved in this mechanism.

Conclusion

We have synthesised size-tunable GQDs (3($\pm$0.3), 5($\pm$0.3), 8.2($\pm$0.3) nm at 90°C, 23($\pm$2) nm at room temperature) for the first time from MWCNTs by an electrochemical approach in a non-aqueous solution without using any molecular capping agent. These quantum dots are especially useful for cellular and molecular imaging applications due to intrinsic luminescence behaviour, higher photostability and enhanced fluorescence quantum yield.

Experimental Section

MWCNTs Nanocyl were dispersed into *N,N*-dimethylforamide (DMF; Aldrich) as received by ultrasonication. The dispersions were filtered and were stable for weeks at a concentration of 4.5 mg L^{-1}. A thin coating of MWCNTs from Nanocyl (50 μL of the MWCNT dispersion in DMF[36–38] drop casted on the working electrode and dried under IR lamp) was prepared on a glassy carbon electrode (2 mm diameter) for use as working electrode, with Pt foil and Pt wire as counter and reference electrodes, respectively. After applying positive potential for different period to the working electrode, followed by subsequent negative potential for corresponding time intervals, the electrodes were sonicated in water, and subsequently, the GQDs were collected and dialysed for several days to fully remove the Li ions and other impurities. These purified GQDs were finally redispersed in deionised water for subsequent characterisation. The above process could be scaled-up by simply using large-area working electrode and extended time. Prior use of acid functionalisation technique has also suggested faster opening of the tips of nanotubes to cause effective intercalation. These GQDs were characterised by a variety of structural and spectroscopic tools as explained in the main text.

[1] A. K. Geim, K. S. Novoselov, *Nat. Mater.* **2007**, *6*, 183.

[2] A. A. Green, M. C. Hersam, *Nano Lett.* **2009**, *9*, 4031.

[3] X. L. Li, X. R. Wang, L. Zhang, S. W. Lee, H. J. Dai, *Science* **2008**, *319*, 1229.

[4] K. S. Novoselov, A. K. Geim, S. V. Morozov, D. Jiang, Y. Zhang, S. V. Dubonos, I. V. Grigorieva, A. A. Firsov, *Science* **2004**, *306*, 666.

[5] L. Y. Jiao, L. Zhang, X. R. Wang, G. Diankov, H. Dai, *Nature* **2009**, *458*, 877.

[6] G. Eda, Y. Y. Lin, C. Mattevi, H. Yamaguchi, H. A. Chen, I. S. Chen, C. W. Chen, M. Chhowalla, *Adv. Mater.* **2010**, *22*, 505.

[7] S. L. Hu, J. Sun, X. W. Du, F. Tian, L. Jiang, *Diamond Relat. Mater.* **2008**, *17*, 142.

[8] S. L. Hu, K. Y. Niu, J. Sun, J. Yang, N. Q. Zhao, X. W. Du, *J. Mater. Chem.* **2009**, *19*, 484.

[9] H. Li, X. He, Y. Liu, H. Huang, S. Lian, S. T. Lee, Z. Kang, *Carbon* **2011**, *49*, 605.

[10] C. N. R. Rao, A. K. Sood, R. Voggu, K. S. Subrahmanyam, *J. Phys. Chem. Lett.* **2010**, *1*, 572.

[11] L. S. Li, X. Yan, *J. Phys. Chem. Lett.* **2010**, *1*, 2572.

[12] S. Coe, W. K. Woo, M. Bavendi, V. Bulovic, *Nature* **2002**, *420*, 800.

[13] Y. Dong, N. Zhou, X. Lin, J. Lin, Y. Chi, G. Chen, *Chem. Mater.* **2010**, *22*, 5895.

[14] V. Gupta, N. Haudhary, R. Srivastava, G. D. Sharma, R. Bhardwaj, S. Chand, *J. Am. Chem. Soc.* **2011**, *133*, 9960.

[15] D. Pan, L. Guo, J. Zhang, C. Xi, Q. Xue, H. Huang, J. Li, Z. Zhang, W. Yu, Z. Chen, Z. Lib, M. Wu, *J. Mater. Chem.* **2012**, *22*, 3314.

[16] Y. Fang, S. Guo, D. Li, C. Zhu, W. Ren, S. Dong, E. Wang, *ACS Nano* **2012**, *6*, 400.

[17] J. Peng, W. Gao, B. K. Gupta, Z. Liu, R. R. Aburto, L. Ge, L. Song, L. B. Alemany, X. Zhan, G. Gao, S. A. Vithayathil, B. A. Kipparettu, A. A. Marti, T. Hayashi, J. Zhu, P. M. Ajayan, *Nano Lett.* **2012**, *12*, 844.

[18] D. Y. Pan, J. C. Zhang, Z. Li, M. H. Wu, *Adv. Mater.* **2010**, *22*, 734.

[19] Y. Li, Y. Hu, Y. Zhao, G. Q. Shi, L. E. Deng, Y. B. Hou, L. T. Qu, *Adv. Mater.* **2011**, *23*, 776.

[20] J. G. Zhou, C. Booker, R. Y. Li, X. T. Zhou, T. K. Sham, X. L. Sun, Z. F. Ding, *J. Am. Chem. Soc.* **2007**, *129*, 744.

[21] R. Liu, D. Wu, X. Feng, K. Müllen, *J. Am. Chem. Soc.* **2011**, *133*, 15221.

[22] L. A. Ponomarenko, F. Schedin, M. I. Katsnelson, R. Yang, E. W. Hill, K. S. Novoselov, A. K. Geim, *Science* **2008**, *320*, 356.

[23] J. Lu, P. S. E. Yeo, C. K. Gan, P. Wu, K. P. Loh, *Nat. Nanotechnol.* **2011**, *6*, 247.

[24] L. Kavan, *Chem. Rev.* **1997**, *97*, 3061.

[25] D. B. Shinde, J. Debgupta, A. Kushwaha, M. Aslam, V. K. Pillai, *J. Am. Chem. Soc.* **2011**, *133*, 4168.

[26] Z. Ding, B. M. Quinn, S. K. Haram, L. E. Pell, B. A. Korgel, A. J. Bard, *Science* **2002**, *296*, 1293.

[27] B. B. L. R. Radovic, *J. Am. Chem. Soc.* **2005**, *127*, 5917.

[28] O. G. D. Bourissou, F. P. Gabba, G. Bertrand, *Chem. Rev.* **2000**, *100*, 39.

[29] R. L. Liu, D. Q. Wu, S. H. Liu, K. Koynov, W. Knoll, Q. Li, *Angew. Chem.* **2009**, *121*, 4668; *Angew. Chem. Int. Ed.* **2009**, *48*, 4598.

[30] A. C. Ferrari, J. Robertson, *Phys. Rev. B* **2000**, *61*, 14095.

[31] A. C. Ferrari, J. Robertson, *Phil. Trans. R. Soc. Lond. A* **2004**, *362*, 2477.

[32] F. Tuinstra, J. L. Koenig, *J. Chem. Phys.* **1970**, *53*, 1126.

[33] L. Bao, Z. Zhang, Z. Tian, L. Zhang, C. Liu, Y. Lin, B. Qi, D. Pang, *Adv. Mater.* **2011**, *23*, 5801.

[34] K. M. J. Wang, Q. Bao, K. P. Loh, *J. Am. Chem. Soc.* **2011**, *133*, 8888.

[35] A. G. Cano-Márquez, F. J. Rodríguez-Macías, J. Campos-Delgado, C. G. Espinosa-González, F. Tristán-López, D. Ramírez-González, D. A. Cullen, D. J. Smith, M. Terrones, Y. I. Vega-Cantú, *Nano Lett.* **2009**, *9*, 1527.

[36] S. Kedem, J. Schmidt, Y. Paz, Y. Cohen, *Langmuir* **2005**, *21*, 5600.

[37] J. Zou, S. I. Khondaker, Q. Huo, L. Zhai, *Adv. Funct. Mater.* **2009**, *19*, 479.

[38] H. Chaturvedi, J. C. Poler, *Appl. Phys. Lett.* **2007**, *90*, 223109.